J. Fluid Mech. (2024), *vol*. 991, A8, doi:10.1017/jfm.2024.546

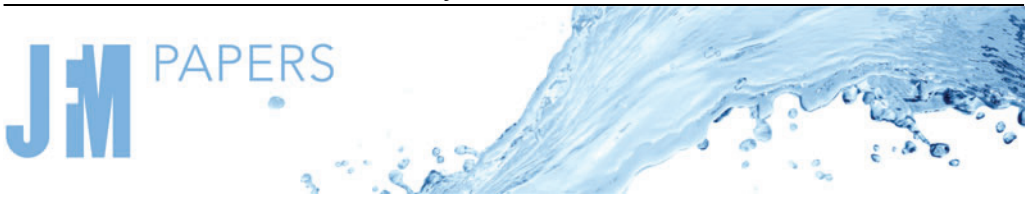

The impact of diffusiophoresis on hydrodynamic dispersion and filtration in porous media

Mamta Jotkar[1,2,†], **Pietro de Anna**[3], **Marco Dentz**[2,†] **and Luis Cueto-Felgueroso**[1]

[1]ETSI Caminos, Canales y Puertos, Universidad Politécnica de Madrid, 28040 Madrid, Spain

[2]Institute of Environmental Assessment and Water Research, Spanish National Research Council, 08034 Barcelona, Spain

[3]Institute of Earth Sciences, Université de Lausanne, 1015 Lausanne, Switzerland

(Received 15 December 2023; revised 29 April 2024; accepted 30 May 2024)

It is known that the dispersion of colloidal particles in porous media is determined by medium structure, pore-scale flow variability and diffusion. However, much less is known about how diffusiophoresis, that is, the motion of colloidal particles along salt gradients, impacts large-scale particle dispersion in porous media. To shed light on this question, we perform detailed pore-scale simulations of fluid flow, solute transport and diffusiophoretic particle transport in a two-dimensional hyper-uniform porous medium. Particles and solute are initially uniformly distributed throughout the medium. The medium is flushed at constant flow rate, and particle breakthrough curves are recorded at the outlet to assess the macroscopic effects of diffusiophoresis. Particle breakthrough curves show non-Fickian behaviour manifested by strong tailing that is controlled by the diffusiophoretic mobility. Although diffusiophoresis is a short-time, microscopic phenomenon owing to the fast attenuation of salt gradients, it governs macroscopic colloid dispersion through the partitioning of particles into transmitting and dead-end pores. We quantify these behaviours by an upscaled analytical model that describes both the retention and release of colloids in dead-end pores and the observed long-time tailings. Our results suggest that diffusiophoresis is an efficient tool to control particle dispersion and filtration through porous media.

Key words: dispersion, porous media, colloids

† Email addresses for correspondence: mmtjotkar@gmail.com, marco.dentz@csic.es

1. Introduction

Natural and engineered porous media are typically characterised by complex porous structures with stagnant flow regions that are not accessible by advection (Bear 1988). Understanding how nano-sized and micro-sized colloidal particles, for example fine powders, contaminants or biological materials, are transported along with nutrients or dissolved solutes through porous media is not only of fundamental interest but also important for technological applications such as groundwater remediation (Kahler & Kabala 2019), the design of water filtration systems (Shin *et al.* 2017; Miele, de Anna & Dentz 2019) and microfluidics for biomedical applications (Rasmussen, Pedersen & Marie 2020).

Diffusiophoresis (DP), that is, the motion of microscopic colloidal particles driven by local gradients of salt concentration (Derjaguin *et al.* 1947), has been demonstrated both theoretically (Prieve *et al.* 1984; Anderson 1989; Velegol *et al.* 2016; Ault, Shin & Stone 2018) and experimentally (Abécassis *et al.* 2008; Palacci *et al.* 2010; Kar *et al.* 2015; Shin *et al.* 2016; Battat *et al.* 2019; Singh *et al.* 2020) as a particle manipulation tool in simple microfluidic set-ups. The physical mechanisms that drive this physicochemical phenomenon can be broken down to two components: chemiphoresis that occurs due the osmotic pressure gradient along the surface of a charged particle (at the scale of the particle) and electrophoresis arising due to the difference in the diffusivities between the cation and the anion in the electrolyte solution (Prieve *et al.* 1984; Anderson 1989; Velegol *et al.* 2016). Note that DP for uncharged colloidal particles occurs via chemiphoresis alone (Derjaguin *et al.* 1947). Diffusiophoresis has been used to induce particle focusing (Shi *et al.* 2016), separation (Shin *et al.* 2017; Shin, Warren & Stone 2018; Rasmussen *et al.* 2020; Jotkar & Cueto-Felgueroso 2021), banding (Staffeld & Quinn 1989) and trapping (Singh *et al.* 2020).

Recent works have studied the impact of DP on colloid transport in microfluidic channels connected to cavities filled with hydrogel (Doan *et al.* 2021; Sambamoorthy & Chu 2023) or biofilm (Somasundar *et al.* 2023), or in a channel connected to a nano-porous medium (Lee *et al.* 2020). In this paper, we focus on more complex geometries in order to assess the impact of DP on hydrodynamic dispersion and particle filtration in disordered porous media. We consider an intricate porous structure characterised by dead-end pores (DEPs) that are connected via a network of percolating channels or transmitting pores (TPs). Such DEP–TP structures lead to anomalous transport of passive tracers (Bordoloi *et al.* 2022). To date, a fundamental understanding of the impact of microscopic interactions of DP and the complexity and disorder of the porous medium on particle transport is missing. We address this question using detailed numerical pore-scale simulations and analytical modelling to elucidate how DP couples with the medium structure to alter macroscopic particle transport. We provide a direct link between the colloidal diffusiophoretic mobility and salt Péclet number to predict, without any fitting parameter, the macroscopic colloidal transport at all times.

2. Numerical simulations

We study a fluid-saturated porous system where a particle suspension gets displaced by a continuously injected salt solution. This particular system mimics a cleanup scenario of an initially contaminated geological or biological porous medium. Nevertheless, the observed transport mechanisms, and the results on particle dispersion, can be transferred to other scenarios. The velocity experienced by each transported particle results from advection in

the flow field $\boldsymbol{u}$, which is controlled by the medium structure and imposed flow rate (Dentz *et al.* 2011; de Anna *et al.* 2017; Dentz, Icardi & Hidalgo 2018), and from DP.

2.1. *Governing equations*

In the thin Debye layer limit, for dilute solutions with valence symmetric mono-valent solutes, that is, for $Z:Z$ electrolytes with $Z=1$, like LiCl and NaCl, the diffusiophoretic drift is proportional to the gradient of the logarithm of the solute concentration s

$$\boldsymbol{u}_{dp} = \Gamma_p \boldsymbol{\nabla} \ln s \tag{2.1}$$

and the diffusiophoretic mobility Γ_p is approximately a constant. For completeness, we mention that in the finite Debye layer limit Γ_p is proportional to the logarithm of the solute concentration (Kirby & Hasselbrink 2004). Here, we consider dilute solutions in the thin Debye layer limit, for which Γ_p is given by (Prieve *et al.* 1984; Anderson 1989)

$$\Gamma_p = \frac{\varepsilon (k_B T)^2}{\mu (Ze)^2} \left\{ \beta \frac{Ze\zeta}{k_B T} + 4 \ln \left[\cosh \left(\frac{Ze\zeta}{4 k_B T} \right) \right] \right\}, \tag{2.2}$$

where ε is the dielectric permittivity of the medium, μ is the dynamic viscosity of the solution, k_B is the Boltzmann constant, T is the absolute temperature, Z is the valence of the constituent ions of the solute, ζ is the zeta potential of the particle, e is the proton charge and $\beta = (D_+ - D_-)/(D_+ + D_-)$ measures the difference in diffusivity D_+ of the cation and D_- of the anion. The prefactor in (2.2) at room temperature is equal to $\varepsilon (k_B T)^2/\mu (Ze)^2 = 470\ \mu\text{m}^2\ \text{s}^{-1}$. Expression (2.2) is valid for valence symmetric $Z:Z$ electrolytes. Note that Γ_p depends implicitly on the particle size because ζ is affected by the absolute surface charge and size of the particle. The logarithmic dependence of the diffusiophoretic drift $\boldsymbol{u}_{dp}$ on the solute concentration gradients $\boldsymbol{\nabla} s$ allows for rapid and efficient particle motion, even in low concentration areas. Positive values of Γ_p refer to upward particle migration along the direction of the concentration gradient, whereas negative values indicate downward migration along the concentration gradient.

In the low Reynolds number limit ($Re \ll 1$), the fluid–solute–particle dynamics is governed by the Stokes equation and the equation of continuity for fluid flow assuming an incompressible fluid

$$-\boldsymbol{\nabla} p + \mu \nabla^2 \boldsymbol{u} = 0, \tag{2.3a}$$

$$\boldsymbol{\nabla} \cdot \boldsymbol{u} = 0, \tag{2.3b}$$

where μ is the dynamic viscosity of the fluid. The advection-diffusion equations for solute and particle transport are (Ault *et al.* 2018)

$$\frac{\partial s}{\partial t} + \boldsymbol{\nabla} \cdot \boldsymbol{u} s = D_s \nabla^2 s, \tag{2.3c}$$

$$\frac{\partial c}{\partial t} + \boldsymbol{\nabla} \cdot (\boldsymbol{u} + \boldsymbol{u}_{dp}) c = D_p \nabla^2 c, \tag{2.3d}$$

where $\boldsymbol{u}$ is the two-dimensional velocity field, p is the pressure, s is the solute concentration and c is the particle concentration, D_s and D_p are the diffusion coefficients of solute and particles. Typically, solutes diffuse much faster than particles such that $D_s \gg D_p$. The volumetric flux through the porous medium is denoted by U such that the average pore velocity is $\bar{u} = U/\phi$. The advection time over the mean pore length λ is defined by

$\tau_v = \lambda/\bar{u}$. We define the dimensionless position vector, pressure, time, velocity, volumetric flux and diffusiophoretic mobility as

$$\boldsymbol{x} = \boldsymbol{x}'\lambda, \quad p = p'\frac{\mu\bar{u}}{\lambda}, \quad t = t'\tau_v, \quad \boldsymbol{u} = \boldsymbol{u}'\bar{u}, \quad U = U'\bar{u}, \quad \Gamma_p = \Gamma_p^* D_s. \tag{2.4a–f}$$

With these definitions, (2.3*a*)–(2.3*d*) can be written as

$$-\nabla' p' + \nabla'^2 \boldsymbol{u}' = 0, \tag{2.5a}$$

$$\boldsymbol{\nabla} \cdot \boldsymbol{u}' = 0, \tag{2.5b}$$

$$\frac{\partial s}{\partial t'} + \nabla' \cdot \boldsymbol{u}' s = \frac{1}{Pe_s}\nabla'^2 s, \tag{2.5c}$$

$$\frac{\partial c}{\partial t'} + \nabla' \cdot \left(\boldsymbol{u}' + \frac{\Gamma_p^*}{Pe_s}\nabla' s\right) c = \frac{1}{Pe_p}\nabla'^2 c, \tag{2.5d}$$

where we used (2.1). The Péclet numbers, $Pe_s = \bar{u}\lambda/D_s$ and $Pe_p = \bar{u}\lambda/D_p$ compare the characteristic diffusion time scales $\tau_{D_s} = \lambda^2/D_s$ and $\tau_{D_p} = \lambda^2/D_p$ with the advection time τ_v. Our study focuses on the interaction of pore-scale heterogeneity and DP while we ignore the interactions between the particles and the solid grains.

2.2. *Porous medium*

We consider a two-dimensional porous medium of length $L = 167\lambda$ and width $W = 100\lambda$ shown in figure 1. The medium characterised by DEPs of different size connected to a network of TPs, was generated using a solid-state de-wetting process (Salvalaglio *et al.* 2020; Bordoloi *et al.* 2022). It exhibits a complex pore structure interspersed among disordered solid grains. The medium is statistically homogeneous with a porosity of $\phi = 0.39$, and a narrow pore-size distribution of mean $\lambda = 30\,\mu\text{m}$. Solutes typically diffuse and dissipate gradients within pores over time scales shorter than the time $\tau_L = L/\bar{u}$ needed to elute a pore volume (also referred to as the mean breakthrough time). The junctures of TPs and DEPs serve as excellent candidates to retain gradients of solute concentration, which in turn trigger DP.

2.3. *Numerical set-up*

The domain is initially saturated with solute at uniform concentration $s_i = 0.1$ mM and particles at uniform concentration $c_i = 0.1$ mM. While c_i may be unrealistically large, the specific value is not important here because particle concentration in the following is normalised by c_i. Thus, the results can be scaled to any desired (more realistic) initial value. Interactions of the particles with the solid matrix are not considered. At time $t > 0$, a sharp front of solute concentration $s_H = 10$ mM is injected such that the ratio $\chi = s_i/s_H = 10^{-2}$. Fluid flow is solved for no-slip boundary conditions at the fluid–solid boundary on the surface of the solid grains (see figure 1), by imposing the constant volumetric flux $U' = \phi$ at the left vertical boundary and constant pressure $p' = 0$ at the right boundary. For the solution of the solute and particle transport equations (2.3*c*) and (2.3*d*), constant flux is imposed at the inlet boundary, and zero gradient at the outlet. We use a finite element scheme to solve for the system of (2.3). For all the simulations shown here, the unstructured mesh is built using 197 723 triangular elements, the maximum size of which is 1×10^{-4} and minimum is 9×10^{-6}. This corresponds to maximum and minimum resolutions of 3.33λ and 0.3λ, respectively. An implicit second-order backward

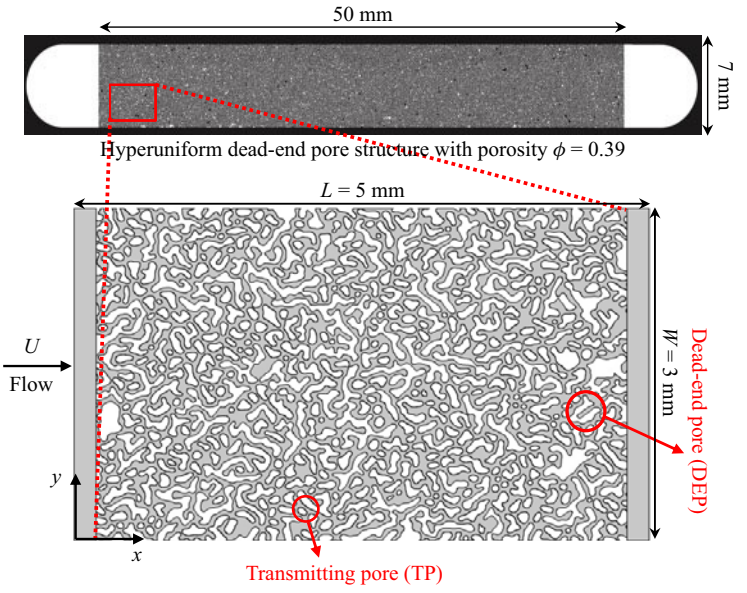

Figure 1. Hyper-uniform porous structure characterised by DEPs and TPs. Computational domain with white spaces indicating solid grains (bottom).

differentiation formulation with adaptive time stepping is used. We have checked that these results are numerically converged by performing simulations with up to 2 695 109 triangular elements with maximum and minimum element sizes of 1×10^{-4} and 6×10^{-6}, respectively.

The dimensionless simulation parameters are listed in table 1. For a realistic solute diffusion coefficient of $D_s = 10^3\ \mu\text{m}^2\ \text{s}^{-1}$, this simulation scenario corresponds to $D_p = 1\ \mu\text{m}^2\ \text{s}^{-1}$, $U = 25\ \mu\text{m}\ \text{s}^{-1}$, $\Gamma_p \in [-1.2, 0.6] \times 10^3\ \mu\text{m}^2\ \text{s}^{-1}$ and valence of the $Z:Z$ electrolyte of $Z = 1$ with a prefactor in (2.2) of $\varepsilon(k_B T)^2/\mu(Ze)^2 = 470\ \mu\text{m}^2\ \text{s}^{-1}$. Note that salt diffusion coefficients are typically of the order of $10^3\ \mu\text{m}^2\ \text{s}^{-1}$, for instance, for LiCl and NaCl, $D_s = 1600\ \mu\text{m}^2\ \text{s}^{-1}$ and $D_s = 1400\ \mu\text{m}^2\ \text{s}^{-1}$, respectively. The value $D_p = 1\ \mu\text{m}^2\ \text{s}^{-1}$ corresponds to spherical colloidal particles with diameters of approximately 500 nm at standard room temperature ($T = 300$ K), according to the Stokes–Einstein relation. To give a few examples, in some of the recent experiments conducted in microfluidic channels (Battat *et al.* 2019; Singh *et al.* 2020), polystyrene colloidal particles were driven by DP arising due to gradients in monovalent solutes like NaCl and LiCl. Typical values for the diffusiophoretic mobility are $|\Gamma_p| \lessapprox 1000\ \mu\text{m}^2\ \text{s}^{-1}$ (Williams *et al.* 2024).

3. Results and discussion

3.1. *Diffusiophoretic particle trapping/extraction*

Figure 2 shows the temporal evolution of the particle concentration field without DP ($\Gamma_p^* = 0$), and for diffusiophoretic trapping ($\Gamma_p^* < 0$), and extraction ($\Gamma_p^* > 0$). In the absence of DP, the majority of the particles get dispersed through the TPs, leaving behind a small fraction of particles that accumulate within the DEPs, where the flow is stagnant, organised in convection rolls and described by closed streamlines (Bordoloi *et al.* 2022).

L	Domain length	167 λ
W	Domain width	100 λ
ϕ	Porosity	0.39
U'	Volumetric flux at inlet	ϕ
Pe_s	Solute Péclet number	1.923
Pe_p	Particle Péclet number	1923
Γ_p^*	Diffusiophoretic mobility	$[-1.2, 0.6]$
$\chi = s_i/s_H$	Initial contrast in the salt concentration imposed	0.01

Table 1. Domain dimensions and parameters used in the numerical simulations.

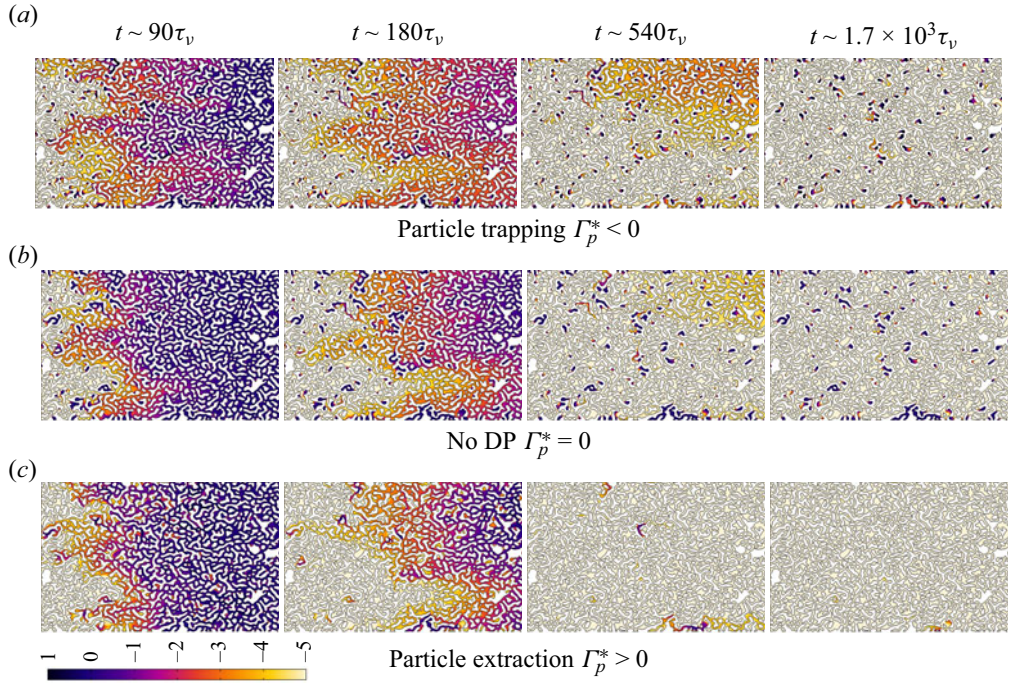

Figure 2. Temporal evolution of the dimensionless particle distributions $\log(c/c_i)$ for (a) trapping, (b) no DP and (c) extraction cases. White spaces indicate solid grains. Flow is from left to right. Note that $\tau_L/\tau_v \approx 167$ such that these plots correspond to times $0.5\tau_L$, $1\tau_L$, $3\tau_L$, and $10\tau_L$, approximately.

The only mechanism through which these localised particles can escape into the TPs is diffusion, the time scale of which is typically orders of magnitude larger than τ_L.

The injection of a sharp front of solute at a higher concentration results in local gradients of solute concentration that drive DP within the DEPs. For $\Gamma_p^* < 0$, that is, when particles migrate from high to low solute concentrations, DP leads to the trapping of particles inside the DEPs, as shown in figure 2(a).

When $\Gamma_p^* > 0$, DP leads to particle mobilisation out of the DEPs because the particles move towards the higher solute concentration zones in the TPs. This is seen in the particle distributions shown in figure 2(c), where the particles within the DEPs rapidly escape the DEPs and leave the domain from the right outlet. Figure 3 shows the time evolution of the solute concentration at a point within a DEP close to the bottom of the DEP. The increase or decrease of concentration due to DP occurs on the time scale τ_{D_s}, which here is smaller

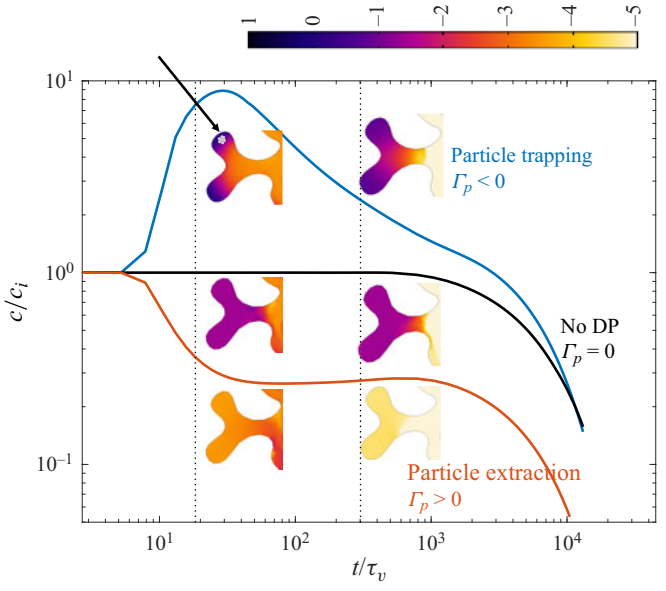

Figure 3. Temporal evolution of dimensionless particle concentration (c/c_i) at an arbitrary point (indicated by the arrow) within a DEP shown in the inset for $\Gamma_p^* < 0$ (blue, trapping), $\Gamma_p^* = 0$ (black, no DP) and $\Gamma_p^* > 0$ (red, extraction). The particle concentrations shown in the inset are the same as in figure 2. Note that time here is non-dimensionalised by τ_v, where $\tau_L/\tau_v \approx 167$.

than τ_{D_p} by a factor of 10^3. Thus, the action of DP on mass transfer between TPs and DEPs is limited to relatively short initial times.

3.2. *Breakthrough curves*

Figure 4(*a*) shows the distribution of arrival times of particles at the outlet, also known as breakthrough curves. Similar to Bordoloi *et al.* (2022), we observe two distinct transport regimes for all the cases. At times of the order of τ_L, particles at the outlet are produced by advection and dispersion from the TPs. For times $t \gg \tau_L$, the arrival time distribution deviates from the exponential decay predicted under the classical dispersion framework (denoted by the dotted curve in figure 4*a*) and displays a power law tailing. This is attributed to the particles that are initially trapped within the DEPs which can only escape the closed streamlines via diffusion, the time scale of which is typically large of the order of $\tau_{D_p} \gg \tau_v$ (here, $Pe = 1923$). For $\Gamma_p^* < 0$, a larger number of particles are trapped initially in the DEP, which manifests in a stronger tailing than the case without DP (indicated by black). For $\Gamma_p^* > 0$, particles are extracted from the DEP at initial times, and thus the tailing is weaker than for $\Gamma_p^* \leq 0$. Note that, albeit unphysical, extreme values of $|\Gamma_p^*|$ are chosen for the breakthrough curves in figure 4(*a*) to demonstrate the exaggerated effects of DP. The range of physically relevant values was discussed earlier in § 2.

The arrival time distribution computed using numerical simulations is predicted analytically by modelling this distribution as the superposition of the residence time distributions in the TPs and DEPs (Bordoloi *et al.* 2022)

$$F(t') = (1-\alpha)F_0(t') + \alpha \int_0^\infty \mathrm{d}\tau \frac{g(t'/\tau)}{\tau} f_D(\tau), \tag{3.1}$$

where α is the effective fraction of particles in the DEPs after particle redistribution due to DP at the short initial time interval, as discussed in the previous section. The first term on

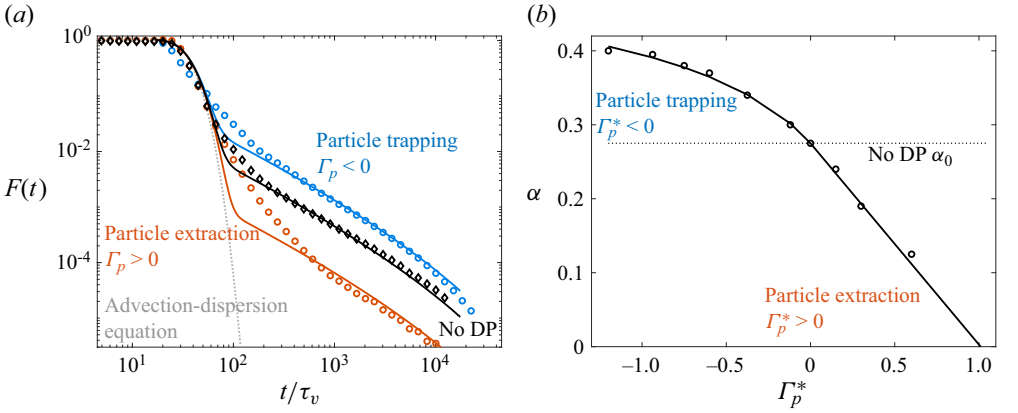

Figure 4. (*a*) Arrival time distribution $F(t)$ at the outlet for (blue circles) $\Gamma_p^* = \Gamma_p/D_s = -1.2$, (black diamonds) 0 and (orange circles) 0.6. The dotted grey line indicates classical prediction under the advection-dispersion framework in (3.2), where the hydrodynamic dispersion is fitted to be $D_h = 7.43$. Solid lines correspond to the travel-time model in (3.1). Note that time here is made dimensionless using τ_v, where $\tau_L/\tau_v \approx 167$. (*b*) Effective trapped particle fraction α in the DEPs from the (symbols) numerical data, and (solid line) the analytical expression (3.7) for $\ell_0^* = 1.6/Pe_p$.

the right side of (3.1) describes transport in the TP by the solution of a one-dimensional advection-dispersion equation characterised by the mean flow velocity $\bar{u} = U/\phi$ and a constant hydrodynamic dispersion coefficient D_h'. The breakthrough curve at $x' = L'$ for a uniform distribution of particles in $0 < x' < \infty$ is then given by (Kreft & Zuber 1978)

$$F_0(t') = 1 - \mathrm{erfc}\left(\frac{L' - U't'/\phi}{\sqrt{4D_h't'}}\right) - \frac{D_h'\phi}{U'}\frac{\exp\left[\dfrac{(L' - U't')^2}{4D_h't'}\right]}{\sqrt{4D_h't'}}. \tag{3.2}$$

The dimensionless hydrodynamic dispersion coefficient is obtained by fitting (3.2) to the numerical data. We find $D_h' = 7.43$. The dimensional dispersion coefficient is given by $D_h = U\lambda D_h'/\phi$. The second term on the right side of (3.1) corresponds to the breakthrough curve of the effective fraction α of particles in DEPs. The function $g(t')$ is given by the Gamma distribution

$$g(t') = \frac{t'^{-2/3}\exp(-t')}{\Gamma(1/3)}, \tag{3.3}$$

which denotes the residence time distribution in a DEP whose characteristic diffusion time is $\tau_\Lambda = 1$. The function $f_D(\tau)$ denotes the distribution of (dimensionless) diffusion times $\tau_\Lambda = \Lambda^2 Pe_p$ within DEPs of (dimensionless) depth Λ, which is obtained from the distribution f_Λ of depths through the map $\Lambda \to \Lambda^2 Pe_p$. Equation (3.1) is used to model the numerical breakthrough curves by adjusting the effective trapped particle fraction α for different values of Γ_p^*.

As we see in figure 4(*a*), expression (3.1) is able to capture the early and late behaviours of the numerical breakthrough curves, but underestimates the arrival time distribution at intermediate times. This is due to the fact that expression (3.2) accounts for heterogeneity in the TPs by a constant hydrodynamic dispersion coefficient. This assumes that the characteristic advection times along TPs are much smaller than the mean arrival time at the outlet. The intermediate tailing observed here indicates that the heterogeneity of the TPs

gives rise to larger advection times. While these effects can be quantified systematically in the framework of continuous time random walks (Dentz *et al.* 2018), we do not account for them in the current model because we focus here on the impact of DP on the long-time tailing of colloids, which is caused by mass transfer between TPs and DEPs. Figure 4(*b*) shows α vs Γ_p^*. For $\Gamma_p^* < 0$ particles are trapped in the DEPs by DP as the medium is flushed. Thus, for $\Gamma_p^* < 0$, α is larger than the trapped particle fraction α_0 for the no-DP case ($\Gamma_p^* = 0$). The tailing of the breakthrough, which is caused by particle retention in DEPs, is stronger than for $\Gamma_p^* = 0$. For $\Gamma_p > 0$, particles are extracted from the DEPs when the medium is flushed. Thus, the effective trapped particle fraction is $\alpha < \alpha_0$. As a consequence, the tailing is weaker than for the no-DP scenario. The physical role of DP is to alter the effective trapped particle fraction α in the DEPs, and thus the tails of the particle breakthrough curves. This behaviour is correctly captured by (3.1).

3.3. *Analytical model to understand how DP controls particle transport*

To understand how DP controls the macroscopic fate of the suspended particles, we now estimate analytically the effective trapped particle fraction α. To this end, we consider a single DEP of length ℓ_p connected to a TP with a width λ. We provide here an outline of the derivation of the analytical model. Further details can be found in the Appendix A. Note that, for clarity, the derivation is in dimensional terms, while the final result for the effective trapped fraction α is again in dimensionless terms.

We assume that particle motion in the DEPs is dominated by the diffusiophoretic drift when the salt gradients are large and represent particle transport by an advection equation. This allows us, by integration, to determine the total mass m_{dp} of particles in the DEPs as a function of the particle concentration $c_0(t)$ and diffusiophoretic drift $u_0(t)$ at the interface between TPs and DEPs

$$m_{dp} = m_i + w \int_0^\infty \mathrm{d}t\, u_0(t) c_0(t), \tag{3.4}$$

where m_i is the initial particle mass and w the width of the interface between TP and DEP. Note that $\alpha = \alpha_0 m_{dp}/m_i$, where α_0 is the effective trapped particle fraction for the no-DP case. In order to determine the diffusiophoretic drift at the interface, we estimate the salt gradient at the interface. We find an analytical solution by using the fact that salt transport in the DEPs is dominated by diffusion. From that and the definition (2.1) of the diffusiophoretic drift, we obtain the expression

$$u_0(t) = -\frac{\Gamma_p(1-\chi)}{\sqrt{4\pi D_s t}} H(\tau_{D_s}\pi - t), \tag{3.5}$$

where $H(t)$ denotes the Heaviside step function and τ_{D_s} is the characteristic salt diffusion time across the DEP. In order to estimate the particle concentration $c_0(t)$ at the interface, we distinguish between particle extraction ($\Gamma_p > 0$) and particle trapping ($\Gamma_p < 0$). In the former case, we set $c_0(t) = c_i$ equal to the resident particle concentration in the TP because the concentration of particles that are advected past the DEPs is constant. In the case of trapping ($\Gamma_p < 0$), this is different. In this case, the particle concentration $c_0(t)$ at the interface is determined by the balance of the diffusive flux of particles from the TP toward the interface, and the diffusiophoretic flux from the interface into the DEP

$$-D_p \frac{c_0(t) - c_i}{\ell_0} = u_0(t) c_0(t). \tag{3.6}$$

The characteristic gradient scale ℓ_0 can be estimated by equating the advective flux past the DEP and the diffusive flux toward it, which gives $\ell_0 \sim D_p/U$. Combining these relations,

we obtain the following expression for α as a function of $\Gamma_p^* = \Gamma_p/D_s$:

$$\alpha = \alpha_0[1 - \Gamma_p^*(1-\chi)] + H(-\Gamma_p^*)\left\{\frac{2\Gamma_p^{*2}(1-\chi)^2 Pe_p \ell_0^*}{\pi Pe_s}\ln\left[\frac{2\Gamma_p^*(1-\chi)Pe_p\ell_0^*}{2\Gamma_p^*(1-\chi)Pe_p\ell_0^* - \pi Pe_s}\right]\right\}. \tag{3.7}$$

The dimensionless gradient scale $\ell_0^* = \ell_0/\lambda$ is inversely proportional to the particle Péclet number such that we set $\ell_0^* = \Sigma/Pe_p$ with Σ a number of order one. The latter is the only fitting parameter of the derived model, which fits the data perfectly for $\Sigma = 1.6$, as shown in figure 4(*b*).

As mentioned above, for positive $\Gamma_p^* > 0$ particles are extracted from the DEPs. In fact, by setting $\alpha = 0$ in expression (3.7), we find that particles are depleted from the DEPs for diffusiophoretic mobilities that are larger than the critical value

$$\Gamma_c^* = 1/(1-\chi), \tag{3.8}$$

as shown in figure 4(*b*), where $\Gamma_c^* \sim 1$. This value corresponds to the extreme case of extraction, where the particles in the DEP will be completely depleted, i.e. when $\alpha = 0$. In the opposite case of negative $\Gamma_p^* < 0$, DP leads to the trapping of particles in the DEPs. As Γ_p^* decreases toward more negative values, the fraction α converges toward the asymptotic value

$$\alpha_\infty = \alpha_0\left(1 + \frac{\pi Pe_s}{\Sigma}\right), \tag{3.9}$$

which is obtained by taking the limit of $\Gamma_p^* \to \infty$. This result shows that the fraction of trapped particles cannot grow without bound. This is due to the fact that, for strongly negative diffusiophoretic mobilities, the rate at which particles are transferred to the interface between TPs and DEPs becomes smaller than the rate at which particles can be transferred into the DEPs by DP. In other words, the supply of particles to the interface is finite and does not increase as Γ_p^* decreases. The analytical model describes the full dependence of α on Γ_p^*, as shown in figure 4(*b*) for both extraction from and trapping in DEPs, and thus seems to correctly capture the controls of DP on the macro-scale dispersion of particles.

4. Conclusions

To summarise, we investigate the effects of diffusiophoresis on particle dispersion in complex porous media. Using pore-scale simulations and analytical modelling, we have quantified the microscopic interactions between DP and flow and transport through porous media to show how this interplay impacts and governs the macroscopic fate of the colloidal particles. More precisely, we have demonstrated how DP occurring locally and microscopically with typically small time scales τ_{D_s}, impacts the macroscopic particle breakthrough curves. We show that the physical role of DP is to alter the effective trapped particle fraction within the DEPs, referred to as α. This is quantified using a novel analytical model derived in (3.7) to give a relation between α and the diffusiophoretic mobility Γ_p. Despite being a localised and short-term phenomenon, DP affects the long-term distribution of the particle arrival times by reorganising the local partitioning of particles between the DEPs and TPs. Depending on the sign of Γ_p, DP can facilitate particle mobilisation out of the DEPs or it may lead to particle entrapment within.

The main implication of our results is that it is possible to access regions in the complex pore space that were initially inaccessible by merely exploiting inherent salt concentration landscapes. This suggests that DP can be used as a tool for controlling particle dispersion and filtration in complex porous media.

The potential of DP to control particle migration in simple microfluidic channels and cavities has been demonstrated and well established in the literature (Shin *et al.* 2016; Lee *et al.* 2020; Singh *et al.* 2020; Somasundar *et al.* 2023). However, despite the ubiquity of engineered and natural porous media in environmental and industrial applications, only little has been known about the impact of DP on macro-scale particle dispersion in complex disordered media. Our work is a first step towards closing this gap by shedding light on the impact of the interaction of DP, medium structure and flow heterogeneity on large-scale particle migration. Therefore, this work not only advances our fundamental understanding but also opens avenues for developing solutions to various technological problems of socio-economic relevance including groundwater remediation and microfluidics for biomedical applications, where DEPs are quite prevalent.

Lastly, it is important to note that this study considers the thin Debye layer limit, and DP that arises from monovalent salts e.g. LiCl and NaCl. In practical scenarios it is likely that the fluid composition is more complex. More investigations are required to understand DP under the influence of multivalent (Wilson *et al.* 2020) multiple salts (Alessio *et al.* 2021) and for finite Debye layer (Kirby & Hasselbrink 2004; Shin *et al.* 2016). In such scenarios, the diffusiophoretic mobility takes a more complex form than the one studied here. Furthermore, the present study does not consider stirring effects arising from diffusioosmosis, that is, bulk flow adjacent to the solid walls of the porous domain, which may be expected if the solid walls are themselves charged. Also, it needs to be pointed out that the model medium under consideration is two-dimensional with explicit dead-end regions. While DEPs in three-dimensional granular media and sphere packs are not likely to occur, they are an important transport-relevant medium property in many three-dimensional porous rocks (Coats & Smith 1964; Fatt, Maleki & Upadhyay 1966) and aggregated media (Philip 1968), and in general in porous materials characterised by a bi-porous structure, such as woven fabrics (Shin *et al.* 2018). Thus, we expect the reported results to be relevant also for particle transport in three-dimensional porous media.

Funding. This work has received funding from European Union's Horizon 2020 research and innovation program under the Marie Skłodowska-Curie G.A. no. 895569. M.D. and L.C.F. gratefully acknowledge funding from the Spanish Ministry of Science and Innovation through the project HydroPore (PID2019-106887GB-C31 and C33). P.d.A. acknowledges the support of FET-Open project NARCISO with grant ID 828890 and of Swiss National Science Foundation G.A. 200021 172587.

Declaration of interests. The authors report no conflict of interest.

Author ORCIDs.
Mamta Jotkar https://orcid.org/0000-0003-1812-0652;
Pietro de Anna https://orcid.org/0000-0002-1492-5755;
Marco Dentz https://orcid.org/0000-0002-3940-282X;
Luis Cueto-Felgueroso https://orcid.org/0000-0001-5303-0236.

Appendix A. Detailed derivation of the analytical model

In this appendix, we elaborate on the derivation of the analytical model described in (3.7), which gives the relation between the initial particle fraction α in the DEPs and the diffusiophoretic mobility Γ_p. The main rationale behind this exercise is that the only mechanism that alters the trapped fraction α of particles within the DEPs is

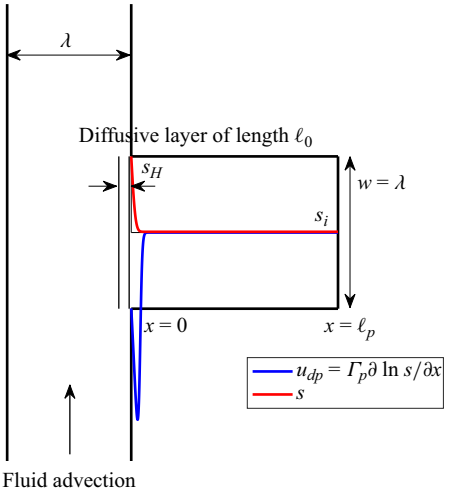

Figure 5. Illustration of the one-dimensional analytical model. A single DEP of length ℓ_p is connected to a (vertical) TP with a width of λ. Typical solute concentration s and diffusiophoretic velocity u_{dp} profiles within the DEP are shown here in red and blue, respectively. At short times, the diffusiophoretic drift is strongly localised at the interface between TP and DEP.

the diffusiophoretic one. Using a simplified one-dimensional model, we first compute the concentration profile and, consequently, the diffusiophoretic drift. Next, a flux balance is performed at the intersection of the DEP and TP after which, an effective trapped particle fraction α is estimated for a given Γ_p.

The arrival time distribution computed numerically for different values of diffusiophoretic mobilities Γ_p is predicted using the one-dimensional statistical model in (3.1) for different effective trapped particle fractions α within the DEPs. This suggests a relation between Γ_p and α (see figure 4).

To understand and quantify this, we construct a one-dimensional model shown in figure 5. We assume that particle transport in the DEP at short times is dominated by the diffusiophoretic drift such that

$$\frac{\partial c}{\partial t} + \frac{\partial}{\partial x} u_{dp} c = 0. \tag{A1}$$

The total mass of particles in the DEP is given by

$$m_{dp} = w \int_0^{\ell_p} \mathrm{d}x\, c, \tag{A2}$$

where w is the pore width. Since the only flux of particles toward or from the DEP is across the DEP–TP junction, the temporal variability of the mass of particles in the DEP is equal to the mass flux at $x = 0$ and controlled by DP. Spatial integration of (A1) according to (A2) gives

$$\frac{\partial m_{dp}}{\partial t} = w u_{dp}(x = 0, t) c(x = 0, t), \tag{A3}$$

where we set $u_0(t) = u_{dp}(x = 0, t)$ and $c_0(t) = c(x = 0, t)$. Note that we used that there is no flux across the boundary at $x = \ell_p$. Thus, the added or extracted mass is given by

$$m_{dp} = m_i + w \int_0^{\infty} \mathrm{d}t\, u_0(t) c_0(t). \tag{A4}$$

In the following, we first determine the diffusiophoretic drift, then we deal with the cases of extraction ($\Gamma_p > 0$) and addition of particles ($\Gamma_p < 0$) separately.

A.1. *Diffusiophoretic drift*

We focus here on estimating the drift u_{dp}. The Péclet number for salt ($Pe_s = 0.75$) is so low that we can assume that diffusion dominates in the DEP. Thus, to obtain the salt concentration s, we solve the diffusion equation

$$\frac{\partial s}{\partial t} - D_s \frac{\partial^2 s}{\partial x^2} = 0. \tag{A5}$$

We consider the boundary conditions $s = s_H$ at $x = 0$ and $\partial s/\partial x = 0$ at $x = L$. The initial condition is $s(x, t = 0) = s_i$. In Laplace space we obtain the exact solution

$$s^*(x, \sigma) = \frac{s_i}{\sigma} + \frac{(s_H - s_i)}{\sigma} \frac{\cosh[(1 - x/\ell_p)\sqrt{\sigma \tau_{D_s}}]}{\cosh(\sqrt{\sigma \tau_{D_s}})}, \tag{A6}$$

where $\tau_{D_s} = \ell_p^2/D_s$ and σ is the Laplace variable. The Laplace transform is defined in Abramowitz & Stegun (1972).

The Laplace transform of the diffusiophoretic velocity at $x = 0$ is then given by

$$u_0^*(\sigma) = -\Gamma_p(1 - \chi) \frac{\tanh(\sqrt{\sigma \tau_{D_s}})}{\sqrt{\sigma D_s}}, \tag{A7}$$

where we defined $\chi = s_i/s_H$. The integral of the drift from $t = 0$ to ∞ is given by

$$\int_0^\infty \mathrm{d}t\, u_0(t) = u_0^*(\sigma = 0) = -\frac{\Gamma_p(1 - \chi)\ell_p}{D_s}. \tag{A8}$$

This expression is used directly to estimate the total mass of trapped particles for the extraction case, as argued below. For the trapping case, however, the full time dependence of $u_0(t)$ is required, as can be seen from (A4). Thus, we approximate the salt concentration profile in the DEP by the solution for a semi-infinite domain

$$s(x, t) = s_i + (s_H - s_i)\,\mathrm{erfc}(x/\sqrt{4D_s t}). \tag{A9}$$

Using this expression, the diffusiophoretic drift is given by

$$u_{dp}(x, t) = -\Gamma_p(s_H - s_i) \frac{\exp(-x^2/4D_s t)}{s(x, t)\sqrt{\pi D_s t}}. \tag{A10}$$

The drift at $x = 0$ then is given by

$$u_0(t) = -\frac{\Gamma_p(1 - \chi)}{\sqrt{\pi D_s t}}, \tag{A11}$$

where we used that $s(x = 0, t) = s_H$. This expression is valid for times larger than $\tau_{D_s} = \ell_p^2/D_s$, after which the salt gradient decays exponentially fast with time. Thus, the time

integral (A8) over the drift can be written in terms of the approximate solution (A11) as

$$-\int_0^{\tau_{D_s} a} \mathrm{d}t\, \frac{\Gamma_p(1-\chi)}{\sqrt{\pi D_s t}} = -\sqrt{\frac{4}{\pi a}}\frac{\Gamma_p(1-\chi)\ell_p}{\sqrt{D_s}}. \tag{A12}$$

In order to match the exact expression (A8), we set $a = \pi/4$ and use the following the approximation:

$$u_0(t) = -\frac{\Gamma_p(1-\chi)}{\sqrt{4\pi D_s t}} H(\tau_{D_s}\pi - t), \tag{A13}$$

where $H(t)$ denotes the Heaviside step function.

A.2. *Extraction of particles*

In the case $\Gamma_p > 0$, particles are extracted from the DEP. The particle concentration at $x = 0$, that is, at the interface with the TP, is set equal to $c_0(t) = c_i$, the resident particle concentration. Thus, we obtain, by integration of (A3), for the added particle mass

$$m_{dp} = m_i + c_i w \int_0^{\infty} \mathrm{d}t\, u_0(t) = m_i + c_i w u_0^*(\sigma = 0) = m_i - \frac{m_i \Gamma_p(1-\chi)}{D_s}, \tag{A14}$$

where $m_i = c_i w \ell_p$ is the initial particle mass and $\chi = s_i/s_H$. Note that we used expression (A8) to arrive at this result. If α_0 is the fraction of particle mass inside the DEP without DP, then the fraction α of particles after DP is

$$\alpha = \alpha_0 \frac{m_{dp}}{m_i}. \tag{A15}$$

Using (A14) and setting $\ell_p = \lambda$ (since the average pore length is approximately equal to the average pore opening in the hyper-uniform porous medium considered), we obtain

$$\alpha = \alpha_0[1 - \Gamma_p^*(1-\chi)], \tag{A16}$$

where $\Gamma_p^* = \Gamma_p/D_s$ is the dimensionless form of the diffusiophoretic mobility.

A.3. *Trapping of particles*

In the case $\Gamma_p < 0$, particles are trapped from the TP into the DEP. In order to determine $c_0(t)$, we consider the balance of fluxes across the interface. For $x < 0$, that is within the TP, the particle flux transverse to the flow direction is due to diffusion. For $x > 0$, that is, in the DEP the particle flux is dominated by the diffusiophoretic drift. Thus, we can write

$$-D_p \frac{c_0(t) - c_i}{\ell_0} = u_0(t) c_0(t), \tag{A17}$$

where ℓ_0 is the concentration gradient scale. We assume that the particle concentration in the flow past the interface between TP and DEP is constant and equal to the initial concentration c_i. We estimate ℓ_0 as the length scale at which the diffusive flux transverse to the flow direction toward the interface is of the same order as the advective flux past the interface, that is,

$$U c_i \sim D_p \frac{c_i}{\ell_0}. \tag{A18}$$

From this relation, we obtain the estimate

$$\ell_0 \sim \frac{D_p}{U} = \frac{\ell_p}{Pe_p}. \tag{A19}$$

That is, particles within the layer of thickness ℓ_0 are available for trapping in the DEP.

From (A17), we obtain for $c_0(t)$

$$c_0(t) = \frac{c_i}{1 + \dfrac{u_0(t)\ell_0}{D_p}}. \tag{A20}$$

Inserting (A20) into (A4) gives

$$m_{dp} = m_i + w \int_0^\infty \mathrm{d}t\, u_0(t) \frac{c_i}{1 + \dfrac{u_0(t)\ell_0}{D_p}}. \tag{A21}$$

Note that, here, we use the approximation (A13) for $u_0(t)$ to derive an analytical expression for m_{dp}.

Inserting expression (A13) into the right side of (A21) gives

$$m_{dp} = m_i - w \int_0^{\tau_{D_s}\pi/4} \mathrm{d}t\, \frac{\Gamma_p(1-\chi)}{\sqrt{\pi D_s t}} \frac{c_i}{1 - \dfrac{\Gamma_p(1-\chi)\ell_0}{\sqrt{\pi D_s t} D_p}}. \tag{A22}$$

We can further write

$$m_{dp} = m_i - w c_i \int_0^{\tau_{D_s}\pi/4} \mathrm{d}t\, \frac{\Gamma_p(1-\chi)}{\sqrt{\pi D_s t} - \dfrac{\Gamma_p(1-\chi)\ell_0}{D_p}}. \tag{A23}$$

Integration of the latter gives

$$m_{dp} = m_i - w\ell_p c_i \left\{ \frac{\Gamma_p(1-\chi)}{D_s} - \frac{2\Gamma_p^2(1-\chi)^2\ell_0}{\pi D_s D_p \ell_p} \ln\left[\frac{2\Gamma_p(1-\chi)}{2\Gamma_p(1-\chi) - \pi D_p \ell_p/\ell_0} \right] \right\}. \tag{A24}$$

Thus, we obtain for α

$$\alpha = \alpha_0 \left\{ 1 - \frac{\Gamma_p(1-\chi)}{D_s} + \frac{2\Gamma_p^2(1-\chi)^2\ell_0}{\pi D_s D_p \ell_p} \ln\left[\frac{2\Gamma_p(1-\chi)}{2\Gamma_p(1-\chi) - \pi D_p \ell_p/\ell_0} \right] \right\}. \tag{A25}$$

We set $\ell_p = \lambda$ and define the dimensionless diffusiophoretic mobility and the dimensionless diffusion layer scale as

$$\Gamma_p^* = \frac{\Gamma_p}{D_s}, \quad \ell_0^* = \frac{\ell_0}{\lambda} \sim 1/Pe_p. \tag{A26a,b}$$

Thus, we can write expression (A26) in dimensionless form as

$$\alpha = \alpha_0 \left\{ 1 - \Gamma_p^*(1-\chi) + \frac{2\Gamma_p^{*2}(1-\chi)^2 Pe_p \ell_0^*}{\pi Pe_s} \ln\left[\frac{2\Gamma_p^*(1-\chi)Pe_p\ell_0^*}{2\Gamma_p^*(1-\chi)Pe_p\ell_0^* - \pi Pe_s} \right] \right\}. \tag{A27}$$

References

Abécassis, B., Cottin-Bizonne, C., Ybert, C., Ajdari, A. & Bocquet, L. 2008 Boosting migration of large particles by solute contrasts. *Nat. Mater.* **7** (10), 785–789.

Abramowitz, M. & Stegun, I.A. 1972 *Handbook of Mathematical Functions*. Dover.

Alessio, B.M., Shim, S., Mintah, E., Gupta, A. & Stone, H.A. 2021 Diffusiophoresis and diffusioosmosis in tandem: two-dimensional particle motion in the presence of multiple electrolytes. *Phys. Rev. Fluids* **6**, 054201.

Anderson, J.L. 1989 Colloid transport by interfacial forces. *Annu. Rev. Fluid Mech.* **21** (1), 61–99.

de Anna, P., Quaife, B., Biros, G. & Juanes, R. 2017 Prediction of velocity distribution from pore structure in simple porous media. *Phys. Rev. Fluids* **2**, 124103.

Ault, J.T., Shin, S. & Stone, H.A. 2018 Diffusiophoresis in narrow channel flows. *J. Fluid Mech.* **854**, 420–448.

Battat, S., Ault, J.T., Shin, S., Khodaparast, S. & Stone, H.A. 2019 Particle entrainment in dead-end pores by diffusiophoresis. *Soft Matter* **15**, 3879–3885.

Bear, J. 1988 *Dynamics of Fluids in Porous Media*. Courier Corporation.

Bordoloi, A.D., Scheidweiler, D., Dentz, M., Bouabdellaoui, M., Abbarchi, M. & de Anna, P. 2022 Structure induced laminar vortices control anomalous dispersion in porous media. *Nat. Commun.* **13**, 3820.

Coats, K.H. & Smith, B.D. 1964 Dead-end pore volume and dispersion in porous media. *Soc. Petrol. Engrs J.* **4** (1), 73–84.

Dentz, M., Icardi, M. & Hidalgo, J.J. 2018 Mechanisms of dispersion in a porous medium. *J. Fluid Mech.* **841**, 851–882.

Dentz, M., Le Borgne, T., Englert, A. & Bijeljic, B. 2011 Mixing, spreading and reaction in heterogeneous media: a brief review. *J. Contam. Hydrol.* **120–121**, 1–17.

Derjaguin, B.V., Sidorenkov, G.P., Zubashchenkov, E.A. & Kiseleva, E.V. 1947 Kinetic phenomena in boundary films of liquids. *Colloid J. USSR* **9**, 335–347.

Doan, V.S., Chun, S.G., Feng, J. & Shin, S. 2021 Confinement-dependent diffusiophoretic transport of nanoparticles in collagen hydrogels. *Nano Lett.* **21** (18), 7625–7630.

Fatt, I., Maleki, M. & Upadhyay, R.N. 1966 Detection and estimation of dead-end pore volume in reservoir rock by conventional laboratory tests. *Soc. Petrol. Engrs J.* **6** (3), 206–212.

Jotkar, M. & Cueto-Felgueroso, L. 2021 Particle separation through diverging nanochannels via diffusiophoresis and diffusioosmosis. *Phys. Rev. Appl.* **16**, 064067.

Kahler, D.M. & Kabala, Z.J. 2019 Acceleration of groundwater remediation by rapidly pulsed pumping: laboratory column tests. *J. Environ. Engng* **145** (1), 06018009.

Kar, A., Chiang, T.-Y., Ortiz Rivera, I., Sen, A. & Velegol, D. 2015 Enhanced transport into and out of dead-end pores. *ACS Nano* **9** (1), 746–753.

Kirby, B.J. & Hasselbrink, E.F. 2004 Zeta potential of microfluidic substrates: 1. Theory, experimental techniques, and effects on separations. *Electrophoresis* **25** (2), 187–202.

Kreft, A. & Zuber, A. 1978 On the physical meaning of the dispersion equation and its solutions for different initial and boundary conditions. *Chem. Engng Sci.* **33** (11), 1471–1480.

Lee, D., Kim, J., Lee, H. & Kim, S.J. 2020 Effect of evaporation through nanoporous medium on diffusiophoresis. *Micro Nano Syst. Lett.* **8**, 1–5.

Miele, F., de Anna, P. & Dentz, M. 2019 Stochastic model for filtration by porous materials. *Phys. Rev. Fluids* **4**, 094101.

Palacci, J., Abécassis, B., Cottin-Bizonne, C., Ybert, C. & Bocquet, L. 2010 Colloidal motility and pattern formation under rectified diffusiophoresis. *Phys. Rev. Lett.* **104**, 138302.

Philip, J.R. 1968 Diffusion, dead-end pores, and linearized absorption in aggregated media. *Soil Res.* **6** (1), 21–30.

Prieve, D.C., Anderson, J.L., Ebel, J.P. & Lowell, M.E. 1984 Motion of a particle generated by chemical gradients. Part 2. Electrolytes. *J. Fluid Mech.* **148**, 247–269.

Rasmussen, M.K., Pedersen, J.N. & Marie, R. 2020 Size and surface charge characterization of nanoparticles with a salt gradient. *Nat. Commun.* **11** (1), 2337.

Salvalaglio, M., *et al.* 2020 Hyperuniform monocrystalline structures by spinodal solid-state dewetting. *Phys. Rev. Lett.* **125**, 126101.

Sambamoorthy, S. & Chu, H.C.W. 2023 Diffusiophoresis of a spherical particle in porous media. *Soft Matter* **19**, 1131–1143.

Shi, N., Nery-Azevedo, R., Abdel-Fattah, A.I. & Squires, T.M. 2016 Diffusiophoretic focusing of suspended colloids. *Phys. Rev. Lett.* **117**, 258001.

SHIN, S., SHARDT, O., WARREN, P.B. & STONE, H.A. 2017 Membraneless water filtration using CO_2. *Nat. Commun.* **8**, 15181.

SHIN, S., UM, E., SABASS, B., AULT, J.T., RAHIMI, M., WARREN, P.B. & STONE, H.A. 2016 Size-dependent control of colloid transport via solute gradients in dead-end channels. *Proc. Natl Acad. Sci.* **113** (2), 257–261.

SHIN, S., WARREN, P.B. & STONE, H.A. 2018 Cleaning by surfactant gradients: particulate removal from porous materials and the significance of rinsing in laundry detergency. *Phys. Rev. Appl.* **9**, 034012.

SINGH, N., VLADISAVLJEVIĆ, G.T., NADAL, F., COTTIN-BIZONNE, C., PIRAT, C. & BOLOGNESI, G. 2020 Reversible trapping of colloids in microgrooved channels via diffusiophoresis under steady-state solute gradients. *Phys. Rev. Lett.* **125**, 248002.

SOMASUNDAR, A., QIN, B., SHIM, S., BASSLER, B.L. & STONE, H.A. 2023 Diffusiophoretic particle penetration into bacterial biofilms. *ACS Appl. Mater Interfaces* **15** (28), 33263–33272.

STAFFELD, P.O. & QUINN, J.A. 1989 Diffusion-induced banding of colloid particles via diffusiophoresis: 1. Electrolytes. *J. Colloid Interface Sci.* **130** (1), 69–87.

VELEGOL, D., GARG, A., GUHA, R., KAR, A. & KUMAR, M. 2016 Origins of concentration gradients for diffusiophoresis. *Soft Matter* **12**, 4686–4703.

WILLIAMS, I., WARREN, P.B., SEAR, R.P. & KEDDIE, J.L. 2024 Colloidal diffusiophoresis in crossed electrolyte gradients: experimental demonstration of an 'action-at-a-distance' effect predicted by the nernst-planck equations. *Phys. Rev. Fluids* **9**, 014201.

WILSON, J.L., SHIM, S., YU, Y.E., GUPTA, A. & STONE, H.A. 2020 Diffusiophoresis in multivalent electrolytes. *Langmuir* **36** (25), 7014–7020.